VOL. 22, NO. 2, 2023, 56-61
elektrika.utm.my
ISSN 0128-4428

ELEKTRIKA
Journal of Electrical Engineering

Substrate Comparison on Multiband Reflector Performance for Intelligent Reflecting Surfaces (IRSs)

Taufiqqurrachman[12*], **Mohamad Kamal B. A. Rahim**[1], **Noor Asmawati Binti Samsuri**[1] and **Yusuf Nur Wijayanto**[2]

[1]Advanced RF and Microwave Research Group (ARFMRG), Faculty of Electrical Engineering, Universiti Teknologi Malaysia, 81310 UTM Skudai, Johor, Malaysia.
[2]National Research and Innovation Agency (BRIN), Bandung, Indonesia.

[*]Corresponding author: taufiqqurrachman@brin.go.id, taufiqqurrachman@gmail.com, mdkamal@utm.my

Abstract: This paper presents the substrate comparison on the multiband reflector performance at X-band frequency for an Intelligent Reflecting Surface (IRS). Functioning as a multiband reflector, the proposed reflector is using a circular multi-ring resonator on several substrates such as RO5880, F4BMX220, RO4003C, and FR4, with slightly different substrate thicknesses based on the available market, that can be operated at X-band frequency. The simulated results have shown in the graph of S-parameters and reflection phase among the substrates. In addition, the bandwidth of the proposed reflector is calculated based on the simulation results. Also, the incident wave angle effect against the proposed reflector is shifted along the horizontal axis. For the overall simulation results, the reflector that uses a RO5880 substrate has slightly better results and a wider bandwidth than the F4BMX220 substrate.

Keywords: Multiband, Reflector, Circular ring resonator, Reflecting Intelligent Surfaces (IRSs)

Article History: received 1 June 2023; accepted 27 August 2023; published 28 August 2023.

1. INTRODUCTION

Reconfigurable Intelligent Surfaces (RISs) are a new wireless transmission technology that enables the concept of smart radio environments in future generations of wireless communication networks. Intelligent Reflecting Surfaces (IRSs) are another term for RISs, which operate as reflectors and allow the phase response of adjustable unit element metasurfaces to be individually modified and optimized for beam-steering, focusing, and other related purposes [1]. Two main types of IRSs used in wireless networks is discussed in [2]. The first form will be implemented into, for example, walls and will be directly controlled by wireless network operators via a software controller in order to shape radio waves for purposes such as boosting network coverage. The second form of IRSs will be embedded in things, such as smart t-shirts with health-monitoring sensors, and will backscatter radio waves generated by cellular base stations in order to report their detected data to mobile phones.

The key research advances of regular metasurfaces and newly designed reconfigurable metasurfaces are examined, with emphasis on the forms of amplitude, phase, polarization, and multi-dimensional modulation as reviewed in [3]. The metasurface that realizes electromagnetic wave amplitude control is primarily utilized to reflect, absorb, or transmit incident electromagnetic wave energy. The phase response properties of the metasurface, on the other hand, are intimately related to the size, shape, rotation mode, and substrate material type of the metasurface unit. The phase difference of transmitted or reflected electromagnetic waves in the orthogonal direction can be realized by creating an asymmetric metasurface unit. All of the aforementioned metasurfaces can only regulate one degree of freedom, such as the amplitude, phase, or polarization of incident electromagnetic waves.

In [4], a metasurface structure is used to enhance a low-profile antenna which is square metal patches on a grounded RO4003 substrate. The proposed metasurface design uses a 4.064 mm of substrate thickness to operate at 2.91 GHz with a 0.72 GHz bandwidth. The proposed reflector has been designed and experimentally demonstrated at 10 GHz for a beamforming metasurface reflector as discussed in [4]. It used a 20x20 unit cells metasurface that consists of two coupled coplanar resonators: an outer split ring resonator (SRR) and an inner dipole ring resonator (DRR). The SRR consists of a tunable capacitance, C_0, and resistance, R, while the DRR consists of a tunable capacitance, C_1. The tunable components are used to control the magnitude and phase separately. This design is fabricated on RO4003C substrate with a thickness of 32 mils. Another proposed reflector structure that uses a 0.254 mm of RO4350B thickness and a gap of 1.8 mm between the RO4350B substrate and ground is shown in [5]. This proposed design is operating

at 80 GHz for an IRS application. Based on [3-4], we can see the difference in thickness and substrate that used in each proposed design which affects the operating frequency and proposed metasurface structure.

The real demonstration of RISs in the sub-6 GHz band has been designed and implemented on an F4BT450 substrate with thicknesses of 1.524 mm where the surfaces is composed of 2430-unit cells [7]. Each unit cell can be controlled by the varactor diodes to set the relative reflection angle of these surfaces. This surface is working properly if the reflection angle of this surface is 15°, 30°, and 45°.

In addition, other metasurfaces for dual band design are reported in [8] and [9]. A dual band metasurface design using a ring resonator with interdigital capacitors is designed to a reflector antenna in [5] where it is suitable to operate for LTE (1.8 GHz) and WiMAX (3.7 GHz). [9] describes a programmable metasurface that combines the benefits of multi-bit phase quantization and dual-band operations (C- and Ku-band). Two PIN diodes are integrated into the radiating element to actively regulate the various functions, and these diodes are controlled by biasing voltage. The 2-bit metasurface featured four states, each with a phase difference of 90° from the next. A dual-frequency channel is presented in the proposed architecture, which can be used for flexible EM wave manipulation, OAM beam creation, holographic imaging, and anomalous reflection. The design method can be applied to transmit-arrays, as well as the terahertz, optical, and acoustic regimes.

This paper proposes a comparison of substrate usage for a multi-band reflector design on X-Band frequency. The substrates used in the proposed reflector are two types of Rogers substrate (RO5880 and RO4003C), F4BMX220, and FR4 substrate. S-parameter, reflection phase, bandwidth, and the effect of the incident wave angle describe the performance of the proposed reflector in terms of substrate usage comparison. It is important to choose and know the best use of substrate for a multi-band reflector design before undertaking the next stage or fabrication stage.

2. Reflector Design

2.1 Multiband Design

A multiband reflector can be easily designed with a multi-ring to produce a multi-resonance frequency. Each ring resonator is designed to produce a resonance frequency using the following equations [11-12]:

For $^{wr}/_{h} \leq 1$,

$$\varepsilon_{re} = \frac{\varepsilon_r+1}{2} + \frac{\varepsilon_r+1}{2}\left(\left(1+12\frac{h}{wr}\right)^{-0.5} + 0.04\left(1-\frac{wr}{h}\right)^{2}\right) \quad (1)$$

$$R = \frac{R_i+R_o}{2} \quad (2)$$

$$f_o(GHz) = \frac{300}{\pi(R_i+R_o)\sqrt{\varepsilon_{re}}} \quad (3)$$

where wr is width line of the circular ring, ε_r is relative permittivity, ε_{re} is effective relative permittivity, h is substrate thickness, R is average radius of the circular ring, R_i and R_o are inner and outer radius of the circular ring.

The geometry of the proposed multiband reflector can be seen in Figure 1. It consists of two layers of the copper sheet which are three circular ring resonators to produce the multi-resonance frequencies at 8, 10, and 12 GHz on the top layer and a full ground plane on the bottom layer to ensure the incoming electromagnetic (EM) wave reflects in one direction. The proposed multiband reflector has been designed on several substrates namely RO5880, RO4003C, F4BMX220, and FR4. Table 1 shows a parameters comparison among four kinds of substrate where RO5880 substrate has a slightly lower loss compared to the others because of the smallest tan δ value and FR4 has a dielectric permittivity (ε_r) value that is greater than the other substrates. The F4BMX220 substrate looks similar to the RO5880 substrate but it has a 0.075 mm difference in the substrate thickness.

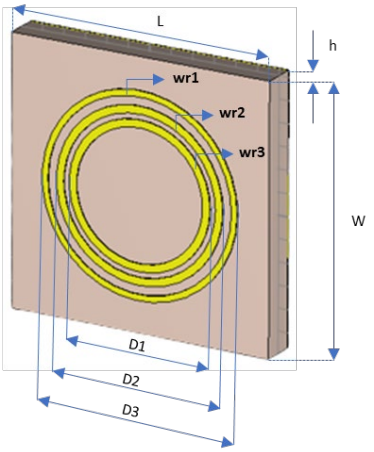

Figure 1. The proposed multiband reflector.

Table 1. Parameters comparison among four kinds of substrate.

Parameters	PCB Substrate			
	RO5880	RO4003C	F4BMX220	FR4
h (mm)	1.575	1.524	1.5	1.6
ε_r	2.2	3.55	2.2	4.3
Tan δ	0.0009	0.0021	0.001	0.01
t (mm)	0.035	0.035	0.035	0.035

Table 2. Dimensional comparison among four kinds of substrates.

Parameters	Substrate			
	RO5880	RO4003C	F4BMX220	FR4
Width of substrate (W)	12	12	12	12
Length of substrate (L)	12	12	12	12
Substrate thickness (h)	1.575	1.575	1.5	1.6
1st ring width (wr1)	0.275	0.35	0.35	0.3
2nd ring width (wr2)	0.346	0.35	0.35	0.315
3rd ring width (wr3)	0.346	0.35	0.35	0.3
1st ring diameter (D1)	9.1	9.112	9.12	7.22
2nd ring diameter (D2)	7.76	7.77	7.756	6.14
3rd ring diameter (D3)	6.57	6.579	6.574	5.2

The overall dimensions of the proposed multiband design on four kinds of substrate are shown in Table 2 and

see Figure 1 where the dimensions differ slightly to achieve the best simulation results on each type of substrate usage. The dimensional differences are caused by the thickness of substrate available in the market for each type of substrate and optimized the coupling effect among the three rings.

2.2 Simulation Results

The simulation results were obtained in the CST Studio Suite for simulating the proposed multiband reflector for each type of substrate. The S-parameters and reflection phase of the proposed multiband reflector among four kinds of substrates are shown in Figure 2. The S-parameters consist of S11 and S21 in the magnitude value where S11 means the reflection value and S21 implies the absorption value.

The reflection value at 8 GHz frequency shows a better value for three kinds of the substrates (RO5880, RO4003C, and F4BMX220), which is 0.9, which means that around 80 % of the incoming EM wave is reflected back. But the reflection values at the 10 and 12 GHz frequencies describes a value above 0.72, which means that the reflected power is approximately 53% reflected back. In the higher frequency, 10 and 12 GHz, the absorption will be even greater due to loss of material from each substrate as shown in Figure 2. a. The absorption is increasing from 0 to 0.24 for all interest frequencies, but the worse value of the absorption is depicted to 10 GHz frequency if using RO4003C substrate, which is 0.24.

While using the FR4 substrate, the reflection value for all the interesting frequency resonances is the worst because the Tan δ has the highest value compared to the other substrates. At 8 GHz, the reflection value has different around 0.46 compared to the others. Then the reflection value at the higher frequency, 10 and 12 GHz, is worse value around 0.4 to 0.5 compared to the others. Furthermore, the absorption value has a higher value at 8 GHz, which is 0.03, but the absorption value at 10 and 12 GHz shows the smallest value compared to the other substrates which means the FR4 substrate cannot absorb the higher frequency.

The reflection phase value of the proposed multiband reflector is described in the graph of the reflection phase as depicted in Figure 2. b. At 8 GHz frequency, the reflection phase shows a phase shift of approximately from 4.41° to 12.24° for all substrates usage. An interesting phenomenon occurs at higher frequency as shown in Table 3, namely 10 and 12 GHz frequencies. If the proposed reflector is using F4BMX220 substrate at 10 GHz frequency, the reflection phase value has a difference of around 18.94° with RO5880 substrate and 22.18° compared with RO4003C substrate. While the reflection phase value at 12 GHz frequency has a difference around 8.07° with RO5880 substrate and 7.07° compared to RO4003C substrate. Furthermore, the reflection phase at 10 and 12 GHz frequencies is out of the specification range if using FR4 substrate, namely 141.39° and 150.33°.

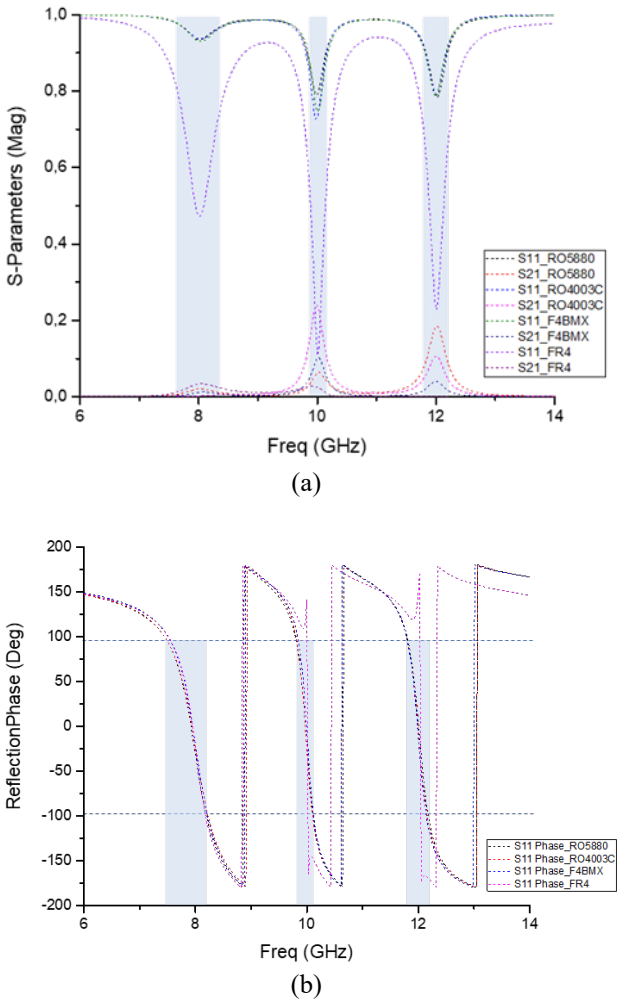

Figure 2. Simulation result among three kinds of the substrate comparison: (a). S-parameters, (b). Reflection phase.

The summaries of the simulated results among four substrates that used in the proposed multiband reflector are shown in Table 3. Based on Figure 2, the bandwidth of the proposed multiband reflector can be determined by using the resonance frequency in the interested frequency and the reflection phase from -90° to +90°. From Table 4, the RO5880 and RO4003C substrates have a wider bandwidth compared to the F4BMX220 substrate. But the FR4 substrate is hard to determine the bandwidth, especially in the higher resonance frequency because the reflection phase is out of the range so that the FR4 substrate is not suitable for the high-frequency design, namely 10 and 12 GHz frequencies.

Table 3. Comparison summaries of simulation results among three kinds of substrate.

Parameters		Substrates			
		RO5880	F4BMX220	RO4003C	FR4
S11 (Mag)	8 GHz	0.93	0.93	0.94	0.47
	10 GHz	0.79	0.75	0.73	0.11
	12 GHz	0.79	0.79	0.79	0.23
S21 (Mag)	8 GHz	0.02	0.012	0.002	0.03
	10 GHz	0.06	0.1	0.24	0.026
	12 GHz	0.18	0.04	0.1	0.0005
Reflection Phase (deg)	8 GHz	-32.35	-20.11	-24.52	-22.95
	10 GHz	-24.14	-5.2	-27.38	141.4
	12 GHz	-5.02	-13.09	-6.02	150.3

Table 4. Bandwidth comparison among three kinds of substrate.

Freq (GHz)	PCB Substrate			
	RO5880	RO4003C	F4BMX220	FR4
8 - BW (GHz)	0.6133	0.64	0.56	0.51
10 - BW (GHz)	0.24	0.24	0.2133	-
12 - BW (GHz)	0.2933	0.2933	0.2667	-

In real conditions, sometimes the planar reflector is located on a wall or huge building to reflect the incoming EM wave to a certain path, but the incoming EM wave is not always pass through in the middle of the planar reflector, assuming in 0°. The next section will only describe the simulated results for three kinds of the substrate usage, RO5880, RO4003C, and F4BMX220, if the incident wave angle is moving from 0° to 72° along the horizontal line as shown in Figures 3 to Figure 5.

2.2.1 The incident wave angle effect if used the RO5880 substrate.

Figure 3 shows the simulated result of the reflection and absorption values for moving the incident wave angle from 0° to 72°. The reflection value at 8 GHz frequency decreased from 0.93 to 0.71 with a slight shift in frequency to a higher frequency and the absorption value at this frequency increased slightly from 0.02 to 0.04. Meanwhile, the reflection values at higher frequencies dropped from 0.79 to 0.42 at 10 GHz frequency and from 0.786 to 0.4 at 12 GHz frequency. The absorption values declined from 0.06 to 0.02 at 10 GHz and from 0.18 to 0.1 at 12 GHz.

Furthermore, the reflection phase value is moving from -32.35° to 128.6° at 8 GHz where if the incident wave angle is 72°, the reflection phase value is out of the specification range. It can be caused by the incident wave not passing through the proposed reflector properly. Meanwhile, the reflection phase value is moving from -24.1° to 24.6° at 10 GHz frequency and from 5° to -42.7° at 12 GHz frequency.

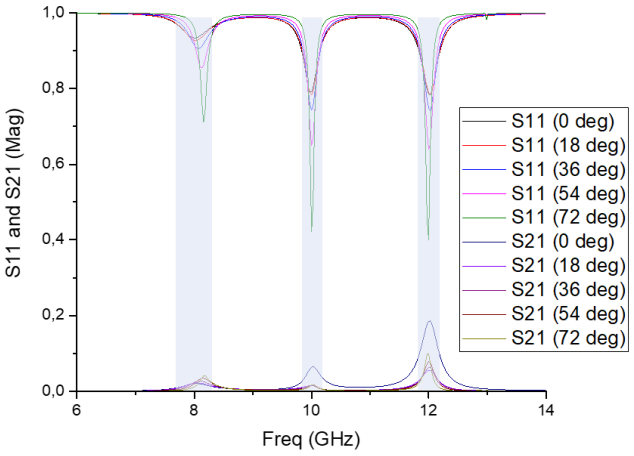

(a)

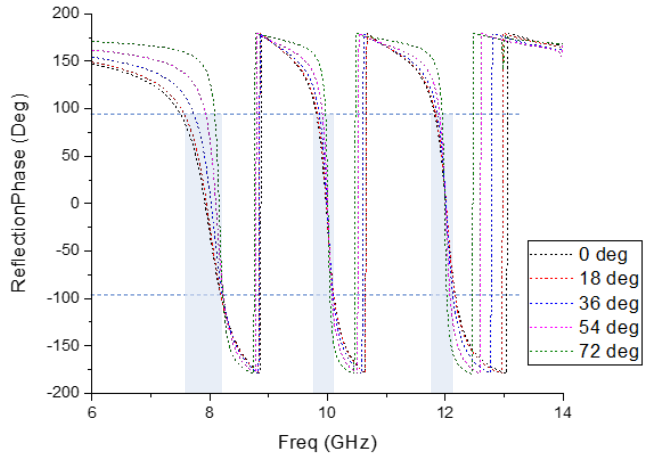

(b)

Figure 3. Incident wave effect from 0 to 72 degrees against the reflector with RO5880 substrate: (a). S-parameters, (b). Reflection phase.

The operating bandwidth of the proposed reflector using RO5880 substrate can be seen clearly in Table 5 where the bandwidth value will be narrowed if the incident wave is moving from 0° to 72°.

Table 5. Bandwidth reduction against the incident wave angle by using RO5880 substrate.

Freq (GHz)	RO5880 PCB Substrate				
	0 deg	18 deg	36 deg	54 deg	72 deg
8 - BW (GHz)	0.61	0.56	0.43	0.27	-
10 - BW (GHz)	0.24	0.24	0.19	0.11	0.05
12 - BW (GHz)	0.29	0.27	0.21	0.13	0.03

2.2.2 The incident wave angle effect if used the RO4003C substrate.

S-parameters and reflection phase graphs of the simulated result based on the incident wave angle effect are shown in Figure 4. In the S-parameters graph, the reflection value will be dropped from 0.94 to 0.72 at 8 GHz frequency with a shifting frequency to the higher frequency. Meanwhile, the reflection value at the higher frequency is moving from 0.73 to 0.26 at 10 GHz and from 0.79 to 0.56 at 12 GHz. But the highest absorption value occurs at 10 GHz, which is 0.32 at the incident wave angle of 72°. It can happen because the incident wave is not properly going through

the proposed reflector so that the reflected power percentage will be dropped. In addition, the reflection phase value at 8 GHz and 12 GHz is shifting from -24.52° to 132.3° and from -6° to -92.3°, respectively, where the reflection phase values at the incident wave angle of 72° are out of the specification range. While the reflection phase value at 10 GHz is shifting from -27.4° to -5.4°.

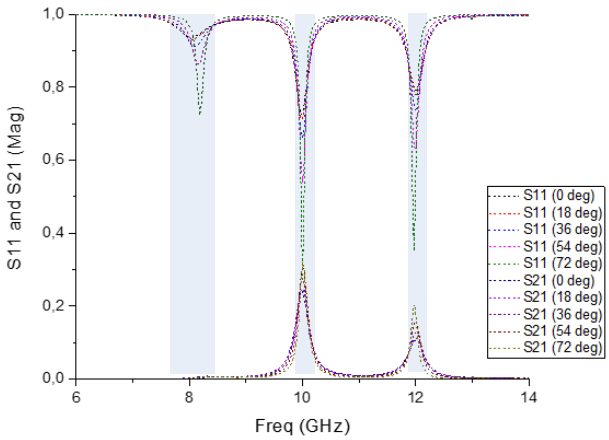

(a)

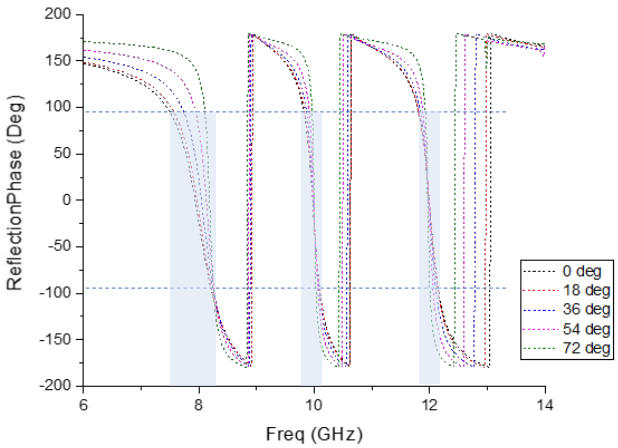

(b)

Figure 4. Incident wave effect from 0 to 72 degrees against the reflector with RO4003C substrate: (a). S-parameters, (b). Reflection phase.

The bandwidth of the proposed reflector using RO4003C can be shown in Table 6. If the incident wave is moving from 0° to 72°, the operating bandwidth of the proposed reflector will be narrowed. But the bandwidth for the incident wave of 72° is hard to determine especially at 8 and 12 GHz because the reflection phase value is out of the specification range.

Table 6. Bandwidth reduction against the incident wave angle by using RO4003C substrate.

Freq (GHz)	RO4003C PCB Substrate				
	0 deg	18 deg	36 deg	54 deg	72 deg
8 - BW (GHz)	0.64	0.56	0.43	0.27	-
10 - BW (GHz)	0.24	0.21	0.16	0.08	0.03
12 - BW (GHz)	0.29	0.27	0.21	0.13	-

2.2.3 The incident wave angle effect if used the F4BMX220 substrate.

Figure 5 shows the simulated result on the F4BMX220 substrate if the incident wave is moving from 0° to 72° where the results are shown in S-parameters and reflection phase graphs. The reflection value at 8 GHz dropped and shifted to a higher frequency from 0.93 to 0.69. While the reflection value is moving from 0.75 to 0.29 at 10 GHz and from 0.79 to 0.39 at 12 GHz where there is a slight shift in frequency. Meanwhile, the higher absorption value has occurred at 10 GHz, which is equal to 0.13 at the incident wave of 72°. Furthermore, the reflection phase value is from -20.1° to 135.9° at 8 GHz and from -13.1° to -106.8° at 12 GHz where the reflection phase values at the incident wave of 72° are out of the specification range. While the reflection phase value at 10 GHz is from -5.2° to 78.8°.

Table 7 shows the operating bandwidth based on the incident wave angle effect. Similar to the other substrates, the operating bandwidth of the proposed reflector will be narrowed. But the operating bandwidth at incident wave of 72° is hard to calculate especially at 8 and 12 GHz.

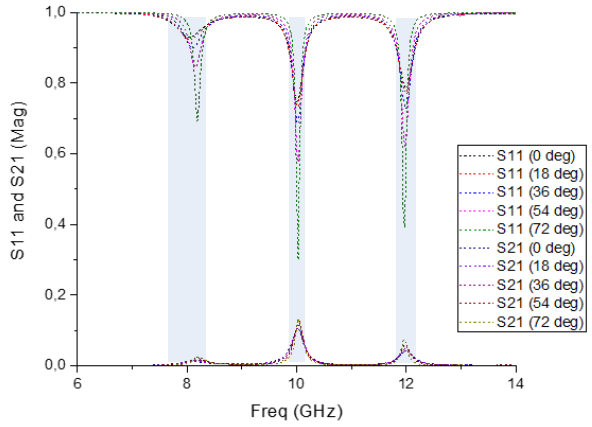

(a)

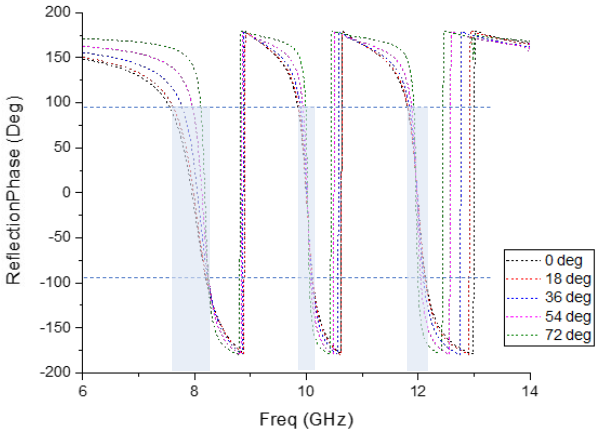

(b)

Figure 5. Incident wave effect from 0 to 72 degrees against the reflector with F4BMX220 substrate: (a). S-parameters, (b). Reflection phase.

Table 7. Bandwidth reduction against the incident wave angle by using F4BMX220 substrate.

Freq (GHz)	F4BMX220 PCB Substrate				
	0 deg	18 deg	36 deg	54 deg	72 deg
8 - BW (GHz)	0.56	0.51	0.4	0.24	-
10 - BW (GHz)	0.21	0.19	0.16	0.08	0.03
12 - BW (GHz)	0.27	0.27	0.21	0.13	-

3. CONCLUSION

For the overall simulated results, the proposed multiband reflector has been designed and simulated by using CST software on several PCB substrates. If the proposed multiband reflector uses the FR4 substrate as a dielectric substrate, the reflection value only reaches lower than 0.5 because the tan δ is too small compared to other substrates and the bandwidth at the higher frequencies is difficult to calculate so that the FR4 substrate is not suitable for the proposed multiband reflector design. The best simulation results can be seen if the proposed design uses the RO5880 substrate because the reflection values at all desired frequencies are slightly better than the RO4003C substrate, especially at 10 GHz. But the RO5880 substrate has an expensive price compared to others. In addition, the proposed reflector can be operated well if the incident wave angle is from 0° to 36° for RO5880, RO4003C, and F4BMX220 substrates.

ACKNOWLEDGMENT

The authors thank the Ministry of Higher Education (MOHE) for supporting the research work under grant FRGS: Ministry of Higher Education under Fundamental Research Grant Scheme, UTM. FRGS/1/2021/TKO/UTM/01/7, Research Management Center (RMC), Universiti Teknologi Malaysia (UTM), Faculty of Electrical Engineering for the support of the research. Also, thanks to the National Research and Innovation Agency (BRIN) for supporting research funding with Rumah Program AI, Big Data, Teknologi Komputasi (AIBDTK) 2023.

REFERENCES

[1] M. Di Renzo et al., "Smart Radio Environments Empowered by Reconfigurable Intelligent Surfaces: How It Works, State of Research, and The Road Ahead," in IEEE Journal on Selected Areas in Communications, vol. 38, no. 11, pp. 2450-2525, Nov. 2020, doi: 10.1109/JSAC.2020.3007211.

[2] Renzo, M.D., Debbah, M., Phan-Huy, DT. et al. Smart radio environments empowered by reconfigurable AI meta-surfaces: an idea whose time has come. J Wireless Com Network 2019, 129 (2019). https://doi.org/10.1186/s13638-019-1438-9.

[3] Zahra S, Ma L, Wang W, Li J, Chen D, Liu Y, Zhou Y, Li N, Huang Y and Wen G (2021) Electromagnetic Metasurfaces and Reconfigurable Metasurfaces: A Review. Front. Phys. 8:593411. doi: 10.3389/fphy.2020.593411.

[4] I. Park, "Application of metasurfaces in the design of performance-enhanced low-profile antennas", EPJ Appl. Metamat. 5, 11 (2018). doi: 10.1051/epjam/2018008.

[5] M. K. Emara, D. Kundu, K. MacDonell, L. M. Rufailand S. Gupta, "Coupled Resonator-Based Metasurface Reflector with Enhanced Magnitude and Phase Coverage". TechRxiv, 14-Apr-2023, doi: 10.36227/techrxiv.22635577.v1.

[6] Barom, A., Rahamim, E., Rozban, D., Rotshild, D. and Abramovich, A., "Millimeter Wave Reconfigurable Metasurface Intelligent Reflection Surface Based on Piezoelectric Crystal for 5th and 6th Generation of Wireless Communication", Communications and Network, 14, 109-118, 2022. https://doi.org/10.4236/cn.2022.144008.

[7] A. Araghi et al., "Reconfigurable Intelligent Surface (RIS) in the Sub-6 GHz Band: Design, Implementation, and Real-World Demonstration," in IEEE Access, vol. 10, pp. 2646-2655, 2022, doi: 10.1109/ACCESS.2022.3140278.

[8] K. Rakdanklang, P. Chomtong, P. Krachodnok and P. Akkaraekthalin, "A Dual-band Metasurface using Ring Resonator with Interdigital Capacitors," 2018 International Symposium on Antennas and Propagation (ISAP), Busan, Korea (South), 2018, pp. 1-2.

[9] Yasir Saifullah, Qinzhuo Chen, Guo-Min Yang, Abu Bakar Waqas, and Feng Xu, "Dual-band multi-bit programmable reflective metasurface unit cell: design and experiment," Opt. Express 29, 2658-2668 (2021), doi: 10.1364/OE.415730.

[10] X. Pei et al., "RIS-Aided Wireless Communications: Prototyping, Adaptive Beamforming, and Indoor/Outdoor Field Trials," in IEEE Transactions on Communications, vol. 69, no. 12, pp. 8627-8640, Dec. 2021, doi: 10.1109/TCOMM.2021.3116151.

[11] J. S. Hong and M. J. Lancaster, "Microstrip filters for RF/Microwave applications," John Wiley & Sons, Inc., New York, 2001.

[12] A. C. Kundu and I. Awai, "Control of attenuation pole frequency of a dual mode microstrip ring resonator bandpass filter," in IEEE Transactions on Microwave Theory and Techniques, vol. 49, no. 6, pp. 1113-1117, June 2001, doi: 10.1109/22.925499